HHS Public Access

Author manuscript

Hepatology. Author manuscript; available in PMC 2022 April 01.

Attenuating the EGFR-ERK-SOX9 axis promotes liver progenitor cell-mediated liver regeneration in zebrafish

Juhoon So[1,*], **Minwook Kim**[1], **Seung-Hoon Lee**[1], **Sungjin Ko**[1,5], **Daniel A. Lee**[2], **Hyewon Park**[3], **Mizuki Azuma**[3], **Michael J. Parsons**[4], **David Prober**[2], **Donghun Shin**[1,*]

[1]Department of Developmental Biology, McGowan Institute for Regenerative Medicine, Pittsburgh Liver Research Center, University of Pittsburgh, Pittsburgh, PA 15260, USA

[2]Division of Biology and Biological Engineering, California Institute of Technology, Pasadena, CA, 91125, USA

[3]Department of Molecular Biosciences, University of Kansas, Lawrence, KS 66045, USA

[4]Department of Developmental and Cell Biology, University of California Irvine, Irvine, CA 92697, USA

[5]Present address: Division of Experimental Pathology, Department of Pathology, University of Pittsburgh School of Medicine, Pittsburgh, PA 15261, USA

Abstract

The liver is a highly regenerative organ, but its regenerative capacity is compromised in severe liver injury settings. In chronic liver diseases, the number of liver progenitor cells (LPCs) correlates proportionally to disease severity, implying that their inefficient differentiation into hepatocytes exacerbates the disease. Moreover, LPCs secrete pro-inflammatory cytokines; thus, their prolonged presence worsens inflammation and induces fibrosis. Promoting LPC-to-hepatocyte differentiation in patients with advanced liver disease, for whom liver transplantation is currently the only therapeutic option, may be a feasible clinical approach since such promotion generates more functional hepatocytes and concomitantly reduces inflammation and fibrosis. Here, using zebrafish models of LPC-mediated liver regeneration, we present a proof-of-principle of such therapeutics by demonstrating a role for the EGFR signaling pathway in differentiation of LPCs into hepatocytes. We found that suppression of EGFR signaling promoted LPC-to-hepatocyte differentiation via the MEK-ERK-SOX9 cascade. Pharmacological inhibition of EGFR or MEK/ERK promoted LPC-to-hepatocyte differentiation as well as genetic suppression of the EGFR-ERK-SOX9 axis. Moreover, Sox9b overexpression in LPCs blocked their differentiation into hepatocytes. In the zebrafish liver injury model, both hepatocytes and biliary epithelial cells contributed to LPCs. EGFR inhibition promoted the differentiation of LPCs regardless of their origin. Notably, short-term treatment with EGFR inhibitors resulted in better liver recovery over the long term.

[*]Correspondence: Donghun Shin, 3501 5th Ave. #5063 Pittsburgh, PA 15260, 1-412-624-2144 (phone), 1-412-383-2211 (fax), donghuns@pitt.edu; Juhoon So, 3501 5th Ave. #5065 Pittsburgh, PA 15260, 1-412-624-2145 (phone), 1-412-383-2211 (fax), juhoon@pitt.edu.

Conclusion: The EGFR-ERK-SOX9 axis suppresses LPC-to-hepatocyte differentiation during LPC-mediated liver regeneration. We suggest EGFR inhibitors as a pro-regenerative therapeutic drug for patients with advanced liver disease.

Keywords

reprogramming; liver progenitor cells; oval cells; biliary epithelial cells; sox9b

Introduction

Although the liver is a highly regenerative organ, its regenerative ability is greatly compromised by prolonged liver damage. Upon mild liver injury, hepatocytes proliferate to restore lost liver mass (1). When hepatocyte proliferation is compromised as in severe liver injury scenarios, however, liver progenitor cells (LPCs) are activated and proceed to proliferate and differentiate into hepatocytes, thereby contributing to regeneration (2, 3). Despite this LPC-mediated mechanism, liver regeneration does not appear to occur efficiently in patients with advanced liver disease, for whom liver transplantation is currently the only therapeutic option (4). In fact, LPC numbers correlate proportionally with the severity of liver disease in humans (5), implying a robust activation of LPCs but inefficient differentiation of LPCs into hepatocytes in patients. Furthermore, LPCs secrete pro-inflammatory cytokines; thus, their prolonged presence exacerbates inflammation and fibrosis (3, 6) and contributes to liver cancer (7). These phenomena suggest that promoting LPC-to-hepatocyte differentiation in patients with advanced liver disease, which generates more functional hepatocytes and concomitantly reduces inflammation and fibrosis, may be a promising therapeutic approach.

The analyses of hepatocyte and biliary marker gene expression in human livers with advanced liver disease have suggested the contribution of biliary epithelial cells (BECs) to hepatocytes through LPCs (8). In addition, recent lineage-tracing studies in zebrafish (9–11) and mice (12–16) have demonstrated the significant contribution of BECs to hepatocytes in severe liver injury settings. Three groups independently reported in zebrafish that near-complete ablation of hepatocytes induces dedifferentiation of BECs into LPCs and subsequent differentiation of LPCs into hepatocytes, thus nearly all regenerated hepatocytes originate from BECs in the zebrafish model (9–11). It was also reported in mice that BECs significantly contribute to regenerated hepatocytes when pre-existing hepatocytes barely proliferate. In these mouse studies, hepatocyte proliferation was blocked genetically by either deleting *Mdm2* (16), *Itgb1* (15), or *Ctnnb1* (12) or overexpressing p21 (15) in hepatocytes. Furthermore, it was reported in mice that without such genetic manipulation, BECs robustly contribute to hepatocytes in severe chronic liver injury settings (13, 14).

These zebrafish and mouse liver injury models can be used to reveal the molecular mechanisms underlying LPC-mediated liver regeneration, which will provide significant insights into developing an effective means to promote this process as pro-regenerative therapeutics. In fact, using the zebrafish model, we and others revealed the essential role of BMP signaling (17), BET proteins (18), Hdac1 (19), mTORC1 (20), and Notch signaling (11, 21) in LPC-mediated liver regeneration. The p21-overexpressing mouse model was also

recently used to reveal the key role of TET1 in the regeneration process (22). Given that upon hepatocyte ablation, LPC-mediated liver regeneration occurs rapidly in the zebrafish model, the model is suitable for identifying compounds that suppress the regeneration process. However, it is not suitable for identifying compounds that promote the process. To identify compounds that can promote LPC-mediated liver regeneration, we have established another zebrafish liver injury model in which LPC-mediated liver regeneration occurs slowly. Using this new model, we present here that suppression of EGFR signaling promotes LPC-mediated liver regeneration, particularly LPC-to-hepatocyte differentiation, via the MEK-ERK-SOX9 cascade. Importantly, our findings suggest EGFR inhibitors as a pro-regenerative therapeutic drug for patients with advanced liver disease.

Experimental procedures

Zebrafish lines

Experiments were performed with approval of the Institutional Animal Care and Use Committee at the University of Pittsburgh. Embryos and adult fish were raised and maintained under standard laboratory conditions (23). We used the following transgenic and mutant lines: *Tg(fabp10a:pt-β-catenin)*^{s704}, *Tg(fabp10a:UHRF1-GFP)*^{mss1a}, *Tg(mpeg1:Dendra2)*^{uwm12}, *Tg(hand2:EGFP)*^{pd24}, *Tg(acta2:mCherry)*^{uto5}, *Tg(fabp10a:GFP)*^{as3}, *Tg(WRE:d2GFP)*^{kyu1}, *Tg(fabp10a:CFP-NTR)*^{s931}, *Tg(Tp1:VenusPEST)*^{s940}, *Tg(Tp1:H2B-mCherry)*^{s939}, *Tg(fabp10a:CreERT2)*^{pt602}, *Tg(Tp1:CreERT2)*^{s959}, *Tg(ubb:loxP-GFP-loxP-mCherry)*^{cz1701}, *Tg(hsp70l:dnHRAS)*^{pd7}, *Tg(fabp10a:rtTA,TRE:Venus-KRAS)*^{pt618}, *Tg(ubb:loxP-CFP-loxP-sox9b-2A-mCherry)*^{jh47}, *Tg(ubb:loxP-CFP-loxP-dnsox9b-2A-mCherry)*^{jh48}, *egfra*^{ct870}, and *sox9b*^{fh313}. Their full names are listed in Table S1.

Compound treatments

Tg(fabp10a:pt-β-catenin) larvae were treated with 0.1% dimethyl sulfoxide (DMSO), 2 μM AG1478, 10 μM LY411575, 10 μM SB431542, 10 μM DMH1, 10 μM cyclopamine, 20 μM U0126, 10 μM LY294002, 3 μM JSI124, or 10 μM erlotinib from 13 to 15 days post-fertilization (dpf) for 48 hours. Fresh compounds were used every 24 hours. The larvae were harvested at 15 dpf for cryostat section or their livers were dissected for quantitative PCR (qPCR). *Tg(fabp10a:UHRF1-GFP)* larvae were treated with 0.1% DMSO or 2 μM AG1478 from 9 to 10 dpf for 24 hours.

Additional methods are available in Supporting Information.

Results

Constitutively active β-catenin or UHRF1 expression in hepatocytes induces liver damage and subsequent LPC-mediated liver regeneration

To identify small molecules that can facilitate LPC-to-hepatocyte differentiation, we first established a new zebrafish model for LPC-mediated liver regeneration in which LPCs slowly differentiate into hepatocytes in response to liver damage. We found that *Tg(fabp10a:pt-β-catenin)*^{s704} larvae, which express the mutated, stable form of Xenopus β-

catenin in hepatocytes under the hepatocyte-specific *fabp10a* promoter (24), exhibit such slow LPC-mediated liver regeneration. It has been known that oncogene overexpression in hepatocytes of the mouse liver induces hepatocyte damage and subsequent senescence and death by inducing p53 and p21 expression (25). Likewise in *Tg(fabp10a:pt-β-catenin)* larvae, we observed an increased hepatic expression of *tp53* and its target genes, *p21* and *mdm2* (Fig. 1A and S1A). *Tg(fabp10a:pt-β-catenin)* larvae also exhibited DNA damage, apoptosis, and senescence in hepatocytes, as assessed by pH2AX, TUNEL, and senescence-associated (SA) β-galactosidase staining, respectively (Fig. 1B, 1C, S1B, and S1C). In chronic liver diseases, hepatocyte damage induces inflammation and subsequent LPC activation and fibrosis (26). As expected, the numbers of macrophages and hepatic stellate cells (HSCs) were greatly increased in *Tg(fabp10a:pt-β-catenin)* livers compared to controls, as assessed by the macrophage, *Tg(mpeg1:Dendra2)*^{uwm12}, and the HSC, *Tg(hand2:EGFP)*^{pd24}, reporter lines, respectively (Fig. S1D and S1E). Liver fibrosis was also observed in *Tg(fabp10a:pt-β-catenin)* larvae but not in the controls, as assessed by anti-Collagen I antibody and the smooth muscle alpha2 actin reporter *Tg(acta2:mCherry)*^{uto5} line (Fig. S1F and S1G).

We further analyzed *Tg(fabp10a:pt-β-catenin)* livers using multiple hepatocyte and BEC markers. To mark BECs and LPCs, we used two Notch reporter lines: *Tg(Tp1:H2B-mCherry)*^{s939}, which expresses H2B-mCherry fusion proteins with a long half-life in the nuclei of BECs/LPCs, and *Tg(Tp1:VenusPEST)*^{s940}, which expresses VenusPEST with a short half-life in their cytoplasm (9). Interestingly, the hepatocyte marker Bhmt was initially expressed in all hepatocytes of the *Tg(fabp10a:pt-β-catenin)* liver; however, its expression was gradually lost and barely detected at 15 dpf (Fig. 1D). The double-positive cells considered to be LPCs, *fabp10a*:CFP^{weak}/*Tp1*:H2B-mCherry^{weak}, appeared from 10 dpf and were abundant at 15 dpf (Fig. 1D). These LPCs were also labeled with Alcama and Anxa4, BEC/LPC markers (Fig. S2A). Intriguingly, Bhmt expression gradually reappeared after 15 dpf; at 20 dpf, small clusters of cells expressed Bhmt; at 30 dpf, ~70% of the liver area was covered by Bhmt^{+} cells (Fig. 1D and 1E), which is suggestive of LPC-mediated hepatocyte regeneration. Bhmt-positive, recovered liver regions at 30 dpf were easily distinguished from Bhmt-negative, dysplastic regions containing *Tp1*:H2B-mCherry^{strong} and *fabp10a*:CFP^{weak}/*Tp1*:H2B-mCherry^{weak} double-positive cells (LPCs) (Fig. 1D). These dysplastic regions contained a large number of macrophages and HSCs and were fibrotic (Fig. S1D–F). qPCR analyses with multiple hepatocyte (*bhmt, ces2, gc, serpina1, tdo2a*) and BEC/LPC (*epcam, her9, krt18, sox9b*) markers (Fig. 1F and S2B) further suggest that LPC-mediated liver regeneration occurs in *Tg(fabp10a:pt-β-catenin)* larvae. Additionally, bile secretion into bile ductules, as assessed by BODIPY C5 staining, was impaired in *Tg(fabp10a:pt-β-catenin)* larvae. However, this defect partially recovered from 30 dpf (Fig. S2C), revealing functional recovery as well.

Given that the transcriptional activity of the *fabp10a* promoter is strong in hepatocytes and weak in LPCs (17), it was expected in *Tg(fabp10a:pt-β-catenin)* livers that *pt-β-catenin* mRNA expression and Wnt/β-catenin activity were initially high but became low at 15 dpf and later recovered in regions containing regenerated hepatocytes. Since *pt-β-catenin* is derived from Xenopus, its in situ probe reveals the mRNA expression of *fabp10a:pt-β-catenin*, but not zebrafish *β-catenin*. Using this probe, we found that *pt-β-catenin* was

expressed in the entire liver of *Tg(fabp10a:pt-β-catenin)* larvae at 10 dpf (Fig. S2D), as expected. Intriguingly, this overall expression pattern was also observed in *Tg(fabp10a:pt-β-catenin)* larvae at 15 dpf (Fig. S2D). However, *pt-β-catenin* was not expressed in the entire liver of *Tg(fabp10a:pt-β-catenin)* larvae at 30 dpf (Fig. S2D, asterisk). These *pt-β-catenin* expression patterns were consistent with the patterns of Wnt/β-catenin activity, which was assessed by the Wnt reporter *Tg(WRE:d2GFP)* line (27). Wnt/β-catenin activity was observed in the entire liver of *Tg(fabp10a:pt-β-catenin)* larvae at 10 and 15 dpf, although *WRE:*d2GFP expression was rather weaker at 15 than 10 dpf (Fig. S2E). In 30-dpf *Tg(fabp10a:pt-β-catenin)* larvae, Wnt/β-catenin activity was not observed in the entire liver (Fig. S2E). Based on Bhmt and *WRE:*d2GFP expression, the 30-dpf liver can be divided into three distinct regions: $Bhmt^{+}/d2GFP^{+}$ (hepatocytes), $Bhmt^{+}/d2GFP^{-}$ (hepatocytes), and $Bhmt^{-}/d2GFP^{-}$ (dysplastic region). The presence of the $Bhmt^{+}/d2GFP^{-}$ region suggests the silence of *fabp10a:pt-β-catenin* transcription in a subset of hepatocytes derived from LPCs.

We hypothesized that hepatocyte-specific overexpression of other oncogenes could also induce hepatocyte damage and subsequent LPC-mediated regeneration, as observed in *Tg(fabp10a:pt-β-catenin)* larvae. Ubiquitin-like with PHD and ring finger domains 1 (UHRF1), a key regulator of DNA methylation, is highly expressed in many cancers and its overexpression in hepatocytes drives DNA hypomethylation, leading to senescence and hepatocellular carcinoma (28). As expected, $Tg(fabp10a:UHRF1\text{-}GFP)^{mss1a}$ larvae, which expresses the human form of UHRF1 fused with GFP in hepatocytes, also exhibited LPC-mediated liver regeneration. Bhmt was initially expressed in all hepatocytes; however, by 10 dpf, its hepatic expression was barely detected (Fig. S3A). On the other hand, *fabp10a:*UHRF1-GFP/*Tp1:*H2B-mCherry/Anxa4 triple-positive cells, which are considered to be LPCs, were prevalent at this stage even though they were not detected earlier at 5 or later at 20 dpf (Fig. S3A and S3B). Liver fibrosis was also observed in *Tg(fabp10a:UHRF1-GFP)* livers (Fig. S3C). Collectively, these data demonstrate the establishment of two liver injury models for LPC-mediated liver regeneration, *Tg(fabp10a:pt-β-catenin)* and *Tg(fabp10a:UHRF1-GFP)*, as characterized by the exhibition of oncogene-induced hepatocyte damage, inflammation and fibrosis, LPC activation, and gradual LPC-to-hepatocyte differentiation.

Both pre-existing hepatocytes and BECs contribute to regenerated hepatocytes in *Tg(fabp10a:pt-β-catenin)* and *Tg(fabp10a:UHRF1-GFP)* zebrafish

Given that both hepatocytes and BECs can give rise to LPCs (12, 14–16, 29, 30), we utilized genetic fate mapping to prospectively determine the origin of regenerated hepatocytes in *Tg(fabp10a:pt-β-catenin)* larvae. The $Tg(Tp1:CreERT2)^{s959}$ and $Tg(fabp10a:CreERT2)^{pt602}$ inducible Cre lines were used to trace BECs and hepatocytes, respectively (9), along with the $Tg(ubb:loxP\text{-}GFP\text{-}loxP\text{-}mCherry)^{cz1701}$ Cre-reporter line (Fig. S4A–D). Intriguingly, we found that both pre-existing BECs and hepatocytes contributed to hepatocytes in 30-dpf *Tg(fabp10a:pt-β-catenin)* larvae (Fig. 2A and 2B). We also observed that pre-existing BECs, but not hepatocytes, contributed to BECs (Fig. 2C and 2D). It has been reported in mice that hepatocytes dedifferentiate into LPCs and that these hepatocyte-derived LPCs differentiate back into hepatocytes during the recovery period (29). Similarly in *Tg(fabp10a:pt-β-catenin)* larvae, pre-existing hepatocytes dedifferentiated into LPCs (Fig. S4E and S4F) and later

differentiated back into hepatocytes (Fig. 2A). We also found that both pre-existing BECs and hepatocytes contributed to hepatocytes via LPCs in 20-dpf *Tg(fabp10a:UHRF1-GFP)* larvae (Fig. S3A, S3B, S4G, S4H).

Suppressing EGFR signaling promotes LPC-to-hepatocyte differentiation

Using the *Tg(fabp10a:pt-β-catenin)* model, we performed a whole-animal small-scale chemical screen to identify compounds that can promote LPC-to-hepatocyte differentiation. We focused on testing signaling pathways implicated in liver development or regeneration by using their specific inhibitors, including AG1478 (EGFR), LY411575 (Notch), SB431542 (TGFβ), DMH1 (BMP), and cyclopamine (Shh). *Tg(fabp10a:pt-β-catenin)* larvae were treated with each inhibitor from 13 to 15 dpf; Bhmt expression was examined at 15 dpf, at which time LPCs are prevalent but hepatocytes are barely present (Fig. 1D). Intriguingly, AG1478 treatment greatly increased the number of $Bhmt^+$ hepatocytes and concomitantly decreased the number of LPCs (Fig. 3A), suggesting that LPC-to-hepatocyte differentiation was enhanced. Consistent with the negative effect of Notch signaling on LPC-to-hepatocyte differentiation (21), LY411575 treatment also increased the number of $Bhmt^+$ hepatocytes, but less effectively than AG1478 (Fig. 3A). The enhanced differentiation by AG1478 was further confirmed with additional hepatocyte and LPC/BEC markers (Fig. 3B, 3C, and S5A). The formation of bile canaliculi and bile secretion into bile ductules, as assessed by Abcb11 expression and BODIPY C5 labeling, respectively, were also improved in AG1478-treated *Tg(fabp10a:pt-β-catenin)* livers (Fig. S5B and S5C). We empirically observed that *Tg(fabp10a:pt-β-catenin)*, but not control, larvae die upon 4-hydroxytamoxifen (4-OHT) treatment beginning at 13 dpf, possibly due to liver toxicity (31). Using this phenomenon, we tested if the improved liver recovery by the temporal AG1478 treatment was beneficial to an animal's survival. 4-OHT treatment from 15 to 16 dpf resulted in ~50% survival of *Tg(fabp10a:pt-β-catenin)* larvae, whereas it resulted in ~80% survival of AG1478-treated *Tg(fabp10a:pt-β-catenin)* larvae (Fig. S5D). Given the role of EGFR signaling in liver fibrosis (32), we also examined fibrosis in AG1478-treated *Tg(fabp10a:pt-β-catenin)* livers. AG1478 treatment reduced liver fibrosis, as assessed by *acta2* and *col1a1a* expression and the *Tg(acta2:mCherry)* line (Fig. S5E). Moreover, we found that *egfra* expression was increased in *Tg(fabp10a:pt-β-catenin)* livers at 15 dpf compared to controls (Fig. 3D). Importantly, $egfra^{ct870}$ heterozygous and homozygous mutants, which survive into adulthood (33), exhibited enhanced LPC-to-hepatocyte differentiation in *Tg(fabp10a:pt-β-catenin)* livers (Fig. 3E and 3F). Altogether, these data demonstrate that suppressing EGFR signaling promotes LPC-to-hepatocyte differentiation and liver recovery.

Suppressing EGFR signaling also promoted LPC-to-hepatocyte differentiation in *Tg(fabp10a:UHRF1-GFP)* larvae. Because of the toxic effect of UHRF1 overexpression, *Tg(fabp10a:UHRF1-GFP)* larvae have micro-livers and most of them die before 20 dpf (28). Yet, AG1478 treatment from 9 to 10 dpf enhanced Bhmt expression in *Tg(fabp10a:UHRF1-GFP)* livers at 10 dpf (Fig. S6A). Additionally, the temporal AG1478 treatment significantly increased the survival of *Tg(fabp10a:UHRF1-GFP)* larvae at 20 dpf (Fig. S6B), supporting the beneficial effect of temporal EGFR inhibition. In the complete hepatocyte-ablation model $Tg(fabp10a:CFP\text{-}NTR)^{s931}$, in which BECs rapidly and robustly contribute to hepatocytes via LPCs upon hepatocyte ablation (9), AG1478 treatment also increased the

hepatic expression of *gc* at R6h (6 hours post-ablation) (Fig. S6C). Although less effective than AG1478 treatment, hepatic *gc* expression at R6h relatively increased in *egfra* mutants compared to wild-type controls (Fig. S6D). Data from these two additional liver injury models further support the positive effect of EGFR inhibition on LPC-to-hepatocyte differentiation.

EGFR inhibition promotes differentiation of both hepatocyte- and BEC-derived LPCs into hepatocytes

Given a mouse study revealing the molecular and functional differences between hepatocyte- and BEC-derived LPCs (29), we next investigated whether EGFR inhibition promoted LPC differentiation regardless of its origin. Hepatocyte- and BEC-derived LPCs were genetically labeled using the *Tg(fabp10a:CreERT2)* and *Tg(Tp1:CreERT2)* lines, respectively, along with the *Tg(ubb:loxP-GFP-loxP-mCherry)* line. AG1478 treatment promoted differentiation of both hepatocyte- and BEC-derived LPCs into hepatocytes in *Tg(fabp10a:pt-β-catenin)* livers, although there was greater differentiation of hepatocyte-derived LPCs than that of BEC-derived LPCs (Fig. 3G).

EGFR signaling suppresses LPC-to-hepatocyte differentiation via the MEK/ERK cascade

Given the pro-regenerative effect of EGFR inhibition, we next sought to identify the molecular mechanisms by which EGFR signaling controls LPC differentiation. EGFR signaling functions via three downstream mediators (34), MEK/ERK, PI3K/AKT and JAK/STAT3. Using their inhibitors (U0126 for MEK/ERK, LY294002 for PI3K/AKT, and JSI-124 for JAK/STAT3), we found that U0126, but not LY294002 or JSI-124, treatment promoted LPC-to-hepatocyte differentiation (Fig. 4A). Consistent with this finding, pErk1/2 expression was greatly reduced in AG1478-treated *Tg(fabp10a:pt-β-catenin)* livers compared with controls (Fig. 4B). Moreover, we confirmed the role of MEK/ERK in LPC differentiation using a genetic tool, *Tg(hsp70l:dnHRAS)*^{pd7}, which overexpresses a dominant-negative version of HRAS (dnHRAS) upon heat-shock. dnHRAS-overexpressing *Tg(fabp10a:pt-β-catenin)* larvae exhibited enhanced LPC-to-hepatocyte differentiation, as assessed by the expression of the hepatocyte markers, Bhmt, *cyp2ad2*, *cyp7a1a*, and *tdo2a* (Fig. 4C and 4D). We further revealed that the effect of EGFR inhibition on LPC differentiation is mediated by MEK/ERK. To do so, we generated a transgenic line, *Tg(fabp10a:rtTA,TRE:Venus-KRAS)*^{pt618}, which expresses a constitutive-active form of human KRAS fused with Venus under the control of the *fabp10a* promoter upon doxycycline treatment. The hepatic induction of KRAS activated Erk1/2, as assessed by pErk1/2 expression, and importantly blocked Bhmt expression in AG1478-treated *Tg(fabp10a:pt-β-catenin)* livers (Fig. 4E). Altogether, these data reveal that EGFR signaling regulates LPC-to-hepatocyte differentiation via the MEK/ERK cascade.

Because prolonged LPCs contribute to inflammation, fibrosis, and liver cancer (3, 6, 7), we investigated whether the temporal inhibition of EGFR and MEK from 13 to 15 dpf, i.e., promotion of LPC-to-hepatocyte differentiation, resulted in a long-term effect at 30 dpf. Particularly, we examined dysplastic regions featured with inflammation and fibrosis in 30-dpf *Tg(fabp10a:pt-β-catenin)* larvae (Fig. 1D and S1D–F). The two-day treatment with AG1478 or erlotinib, another EGFR inhibitor used in clinics, greatly increased liver area

covered by Bhmt$^+$ hepatocytes and simultaneously reduced dysplastic regions devoid of hepatocytes in 30-dpf *Tg(fabp10a:pt-β-catenin)* larvae (Fig. 4F). The increased hepatocyte area by the two-day AG1478 treatment was also confirmed by the expression of two additional hepatocyte markers, *ces3* and *gc* (Fig. 4G). As expected, U0126 treatment also increased Bhmt$^+$ liver area and reduced dysplastic regions (Fig. 4F). These data further support the key role of the EGFR-MEK-ERK axis in LPC-to-hepatocyte differentiation and suggest the benefits of enhancing LPC-to-hepatocyte differentiation in chronic liver diseases.

EGFR signaling suppresses LPC-to-hepatocyte differentiation through Sox9b.—SOX9 is known to maintain the stem cell/progenitor state and inhibit their differentiation in various tissues (35–37). In zebrafish, we recently reported that Sox9b represses LPC-to-hepatocyte differentiation in the complete hepatocyte-ablation model (19, 21). Since EGFR signaling via MEK/ERK induces SOX9 expression in urothelial cells (38) and glioblastoma (39), we hypothesized that Sox9b might play a role as a key downstream effector of EGFR signaling in LPC-mediated liver regeneration. Sox9b was highly expressed in *Tg(fabp10a:pt-b-catenin)* livers, but AG1478 treatment greatly reduced this expression (Fig. 5A and 5B). Consistent with the role of the EGFR-ERK axis in LPC differentiation, the hepatic induction of KRAS with the *Tg(fabp10a:rtTA,TRE:Venus-KRAS)* line blocked the effect of EGFR inhibition on Sox9b expression in AG1478-treated *Tg(fabp10a:pt-β-catenin)* livers (Fig. 5C). Importantly, overexpression of Sox9b with the *Tg(ubb:loxP-CFP-loxP-sox9b-2A-mCherry)*^{ih47} and *Tg(fabp10a:CreERT2)* lines abolished the effect of AG1478 treatment on LPC-to-hepatocyte differentiation in *Tg(fabp10a:pt-β-catenin)* larvae (Fig. 5D). Moreover, *sox9b*^{fh313} heterozygous mutants exhibited enhanced LPC-to-hepatocyte differentiation at 15 dpf (Fig. 5E and 5F) and increased Bhmt$^+$ liver area with reduced Bhmt$^-$ dysplastic regions at 30 dpf (Fig. 5E and 5G). To determine if Sox9b suppresses LPC-to-hepatocyte differentiation cell-autonomously, we manipulated Sox9b activity in LPCs using the *Tg(ubb:loxP-CFP-loxP-dnsox9b-2A-mCherry)*^{ih48} and *Tg(ubb:loxP-CFP-loxP-sox9b-2A-mCherry)* lines, which express dominant-negative Sox9b (dnSox9b) and Sox9b, respectively, upon Cre-mediated excision of the CFP-STOP cassette (40). Most dnSox9b/mCherry-positive cells in 15-dpf *Tg(fabp10a:pt-β-catenin)* livers were Bhmt$^+$, whereas most Sox9b/mCherry-positive cells in 20-dpf *Tg(fabp10a:pt-β-catenin)* livers were Bhmt$^-$ (Fig. 5H and 5I), which is indicative of the cell-autonomous effect of Sox9b on LPC differentiation. Altogether, these data reveal that EGFR signaling regulates LPC-to-hepatocyte differentiation through Sox9b.

Discussion

In this study, we developed a new zebrafish model for LPC-mediated liver regeneration in which the regeneration process occurs slowly. Using this new model, we identified EGFR inhibitors as potent compounds that can promote LPC-mediated liver regeneration, particularly LPC-to-hepatocyte differentiation. We also revealed that EGFR signaling regulates this differentiation process through the ERK-SOX9 axis. Given the prevalence of LPCs in diseased human livers, our findings suggest EGFR inhibitors as a pro-regenerative drug for patients with advanced liver disease.

EGFR signaling is known to play a positive role in hepatocyte-mediated liver regeneration by promoting hepatocyte proliferation (41, 42). It also protects hepatocytes in diverse liver injury settings (32). However, we found that EGFR signaling plays a negative role in LPC-mediated liver regeneration: it suppresses LPC-to-hepatocyte differentiation. Notably, it was reported that in a DDC-induced liver damage mouse model, liver-specific *Egfr* conditional knockout mice exhibited better liver function and contained more A6/HNF4A double-positive cells than controls (43). Since these double-positive cells can be considered LPCs that are differentiating into hepatocytes, the finding from the mouse study suggests that LPC-to-hepatocyte differentiation is enhanced in the *Egfr* knockout mice (43), consistent with our findings in zebrafish.

EGFR signaling also regulates HSC activation, thereby contributing to liver fibrosis (32). In the rodent models of liver injury induced by diethylnitrosamine, carbon tetrachloride, and bile duct ligation, erlotinib administration attenuated liver fibrosis (44). We also observed reduced fibrosis in our zebrafish model (Fig. S5E). Given the potent anti-fibrogenic effect of EGFR inhibitors, it could be assumed that reduced fibrosis by EGFR inhibition might secondarily induce LPC-to-hepatocyte differentiation in *Tg(fabp10a:pt-β-catenin)* larvae. However, suppressing fibrosis with the TGFβR inhibitor SB431542 failed to promote LPC-to-hepatocyte differentiation (Fig. 3A), suggesting that there are independent effects of EGFR inhibitors on LPCs from HSCs. Given that LPCs secrete pro-inflammatory cytokines (6, 45, 46), EGFR inhibitors can suppress liver fibrosis directly by inhibiting HSC activation and indirectly by reducing LPC number through its differentiation into hepatocytes.

Notch signaling induces LPC-to-BEC differentiation, but suppresses LPC-to-hepatocyte differentiation during LPC-mediated liver regeneration (11, 19, 47). Using the zebrafish hepatocyte ablation model, we recently reported that suppressing Notch signaling promotes LPC-to-hepatocyte differentiation (21). We also observed that Notch inhibition promoted the differentiation in *Tg(fabp10a:pt-β-catenin)* larvae. However, this promotion was much weaker than that induced by EGFR inhibitors. LY411575-treated *Tg(fabp10a:pt-β-catenin)* larvae exhibited much weaker expression of Bhmt and other hepatocyte markers than AG1478-treated *Tg(fabp10a:pt-β-catenin)* larvae (Fig. 3A and data not shown). This difference also reinforces EGFR inhibitors as a promising, pro-regenerative drug to promote differentiation of LPCs into hepatocytes.

Currently, EGFR inhibitors are used in clinics for patients with non-small-cell lung cancer harboring EGFR activating mutation (48). Despite this anti-tumorigenic effect of EGFR inhibitors, when erlotinib, one such EGFR inhibitor, was administered after tumor formation, tumor growth in a DEN-induced liver cancer model was not reduced (44). However, it reduced tumor incidence when given before tumor formation (44), suggesting that there is an anti-tumorigenic effect of EGFR inhibitors on cells in a precancerous state. Given that prolonged LPCs contribute to inflammation, fibrosis, and cancer (3, 6, 7), the erlotinib data can be explained by the effect of erlotinib on LPCs. Namely, enhanced LPC-to-hepatocyte differentiation reduces the number of prolonged LPCs, which contribute to tumor formation, thereby reducing tumor incidence. Supporting this explanation, we also observed that AG1478 or erlotinib treatment greatly reduced LPC-enriched dysplastic

regions, which will eventually give rise to cholangiocarcinoma, in *Tg(fabp10a:pt-β-catenin)* larvae (Fig. 4F).

In conclusion, we provide evidence that the EGFR-ERK-SOX9 axis suppresses LPC-to-hepatocyte differentiation during LPC-mediated liver regeneration. Given the beneficial effects of EGFR inhibitors on diseased livers, we suggest EGFR inhibitors as a pro-regenerative therapeutic drug for patients with advanced liver disease.

Supplementary Material

Refer to Web version on PubMed Central for supplementary material.

Acknowledgements

We thank Kirsten Sadler for *Tg(fabp10a:UHRF1-GFP),* Alex Nechiporuk and Ken Poss for *Tg(hsp70l:dnHRAS),* Sarah Child for *Tg(acta2:mCherry),* and Anna Huttenlocher for *Tg(mpeg1:Dendra2)* fish. We also thank Jinrong Peng for anti-Bhmt and anti-p53 antibodies, Junsu Kang for the *I-SceI* destination vector, Paul Monga, Sucha Singh, and Jackie Russell for help in H&E staining, Neil Hukriede and Michael Tsang for discussion, and George Michalopoulos, Dean Yimlamai, Andy Duncan, and Angie Kim for critical reading of the manuscript.

Financial Support: The work was supported by NIH grants to D.S. (DK101426, DK116993) and by the NIH/NIDDK Digestive Disease Research Core Center grant P30DK120531.

List of abbreviations:

LPC	liver progenitor cell
BEC	biliary epithelial cell
DMSO	dimethyl sulfoxide
dpf	days post-fertilization
qPCR	quantitative polymerase chain reaction
HSC	hepatic stellate cell
UHRF1	ubiquitin-like with PHD and ring finger domains 1
4-OHT	4-hydroxytamoxifen
dnHRAS	dominant-negative HRAS
dnSox9b	dominant-negative Sox9b

References

1. Michalopoulos GK. Liver regeneration. J Cell Physiol 2007;213:286–300. [PubMed: 17559071]
2. Forbes SJ, Newsome PN. Liver regeneration - mechanisms and models to clinical application. Nat Rev Gastroenterol Hepatol 2016;13:473–485. [PubMed: 27353402]
3. Ko S, Russell JO, Molina LM, Monga SP. Liver Progenitors and Adult Cell Plasticity in Hepatic Injury and Repair: Knowns and Unknowns. Annu Rev Pathol 2019.
4. Kim PT, Testa G. Living donor liver transplantation in the USA. Hepatobiliary Surg Nutr 2016;5:133–140. [PubMed: 27115007]

5. Lowes KN, Brennan BA, Yeoh GC, Olynyk JK. Oval cell numbers in human chronic liver diseases are directly related to disease severity. Am J Pathol 1999;154:537–541. [PubMed: 10027411]
6. Lukacs-Kornek V, Lammert F. The progenitor cell dilemma: Cellular and functional heterogeneity in assistance or escalation of liver injury. J Hepatol 2017.
7. Saha SK, Parachoniak CA, Ghanta KS, Fitamant J, Ross KN, Najem MS, Gurumurthy S, et al. Mutant IDH inhibits HNF-4 alpha to block hepatocyte differentiation and promote biliary cancer (vol 513, 110, 2014). Nature 2015;528:152–152.
8. Stueck AE, Wanless IR. Hepatocyte buds derived from progenitor cells repopulate regions of parenchymal extinction in human cirrhosis. Hepatology 2015;61:1696–1707. [PubMed: 25644399]
9. Choi TY, Ninov N, Stainier DY, Shin D. Extensive conversion of hepatic biliary epithelial cells to hepatocytes after near total loss of hepatocytes in zebrafish. Gastroenterology 2014;146:776–788. [PubMed: 24148620]
10. He J, Lu H, Zou Q, Luo L. Regeneration of liver after extreme hepatocyte loss occurs mainly via biliary transdifferentiation in zebrafish. Gastroenterology 2014;146:789–800.e788. [PubMed: 24315993]
11. Huang MB, Chang A, Choi M, Zhou D, Anania FA, Shin CH. Antagonistic Interaction Between Wnt and Notch Activity Modulates the Regenerative Capacity of a Zebrafish Fibrotic Liver Model. Hepatology 2014;60:1753–1766. [PubMed: 24995814]
12. Russell JO, Lu WY, Okabe H, Abrams M, Oertel M, Poddar M, Singh S, et al. Hepatocyte-Specific beta-Catenin Deletion During Severe Liver Injury Provokes Cholangiocytes to Differentiate Into Hepatocytes. Hepatology 2019;69:742–759. [PubMed: 30215850]
13. Manco R, Clerbaux LA, Verhulst S, Bou Nader M, Sempoux C, Ambroise J, Bearzatto B, et al. Reactive cholangiocytes differentiate into proliferative hepatocytes with efficient DNA repair in mice with chronic liver injury. J Hepatol 2019;70:1180–1191. [PubMed: 30794890]
14. Deng X, Zhang X, Li W, Feng RX, Li L, Yi GR, Zhang XN, et al. Chronic Liver Injury Induces Conversion of Biliary Epithelial Cells into Hepatocytes. Cell Stem Cell 2018;23:114–122.e113. [PubMed: 29937200]
15. Raven A, Lu WY, Man TY, Ferreira-Gonzalez S, O'Duibhir E, Dwyer BJ, Thomson JP, et al. Cholangiocytes act as facultative liver stem cells during impaired hepatocyte regeneration. Nature 2017;547:350–354. [PubMed: 28700576]
16. Lu WY, Bird TG, Boulter L, Tsuchiya A, Cole AM, Hay T, Guest RV, et al. Hepatic progenitor cells of biliary origin with liver repopulation capacity. Nat Cell Biol 2015;17:971–983. [PubMed: 26192438]
17. Choi TY, Khaliq M, Tsurusaki S, Ninov N, Stainier DYR, Tanaka M, Shin D. Bone morphogenetic protein signaling governs biliary-driven liver regeneration in zebrafish through tbx2b and id2a. Hepatology 2017;66:1616–1630. [PubMed: 28599080]
18. Ko S, Choi TY, Russell JO, So J, Monga SP, Shin D. Bromodomain and extraterminal (BET) proteins regulate biliary-driven liver regeneration. J Hepatol 2016;64:316–325. [PubMed: 26505118]
19. Ko S, Russell JO, Tian J, Gao C, Kobayashi M, Feng R, Yuan X, et al. Hdac1 Regulates Differentiation of Bipotent Liver Progenitor Cells During Regeneration via Sox9b and Cdk8. Gastroenterology 2019;156:187–202.e114. [PubMed: 30267710]
20. He J, Chen J, Wei X, Leng H, Mu H, Cai P, Luo L. mTORC1 Signaling is Required for the Dedifferentiation from Biliary Cell to Bi-potential Progenitor Cell in Zebrafish Liver Regeneration. Hepatology 2019.
21. Russell JO, Ko S, Monga SP, Shin D. Notch Inhibition Promotes Differentiation of Liver Progenitor Cells into Hepatocytes via sox9b Repression in Zebrafish. Stem Cells Int 2019;2019:8451282. [PubMed: 30992706]
22. Aloia L, McKie MA, Vernaz G, Cordero-Espinoza L, Aleksieva N, van den Ameele J, Antonica F, et al. Epigenetic remodelling licences adult cholangiocytes for organoid formation and liver regeneration. Nat Cell Biol 2019.
23. Westerfield M The Zebrafish Book: A Guide for the Laboratory Use of Zebrafish (Danio rerio): University of Oregon Press, 2000.

24. Evason KJ, Francisco MT, Juric V, Balakrishnan S, Lopez Pazmino Mdel P, Gordan JD, Kakar S, et al. Identification of Chemical Inhibitors of beta-Catenin-Driven Liver Tumorigenesis in Zebrafish. PLoS Genet 2015;11:e1005305. [PubMed: 26134322]
25. Xue W, Zender L, Miething C, Dickins RA, Hernando E, Krizhanovsky V, Cordon-Cardo C, et al. Senescence and tumour clearance is triggered by p53 restoration in murine liver carcinomas. Nature 2007;445:656–660. [PubMed: 17251933]
26. Williams MJ, Clouston AD, Forbes SJ. Links between hepatic fibrosis, ductular reaction, and progenitor cell expansion. Gastroenterology 2014;146:349–356. [PubMed: 24315991]
27. Shimizu N, Kawakami K, Ishitani T. Visualization and exploration of Tcf/Lef function using a highly responsive Wnt/beta-catenin signaling-reporter transgenic zebrafish. Dev Biol 2012;370:71–85. [PubMed: 22842099]
28. Mudbhary R, Hoshida Y, Chernyavskaya Y, Jacob V, Villanueva A, Fiel MI, Chen X, et al. UHRF1 overexpression drives DNA hypomethylation and hepatocellular carcinoma. Cancer Cell 2014;25:196–209. [PubMed: 24486181]
29. Tarlow BD, Pelz C, Naugler WE, Wakefield L, Wilson EM, Finegold MJ, Grompe M. Bipotential adult liver progenitors are derived from chronically injured mature hepatocytes. Cell Stem Cell 2014;15:605–618. [PubMed: 25312494]
30. Yanger K, Zong Y, Maggs LR, Shapira SN, Maddipati R, Aiello NM, Thung SN, et al. Robust cellular reprogramming occurs spontaneously during liver regeneration. Genes Dev 2013;27:719–724. [PubMed: 23520387]
31. Gao FF, Lv JW, Wang Y, Fan R, Li Q, Zhang Z, Wei L. Tamoxifen induces hepatotoxicity and changes to hepatocyte morphology at the early stage of endocrinotherapy in mice. Biomed Rep 2016;4:102–106. [PubMed: 26870344]
32. Komposch K, Sibilia M. EGFR Signaling in Liver Diseases. Int J Mol Sci 2016;17.
33. Lee DA, Liu J, Hong Y, Hou S, Hill AJ, Lane JM, Wang H, et al. Evolutionarily Conserved Regulation of Sleep by Epidermal Growth Factor Receptor Signaling. Science Advances 2019;in press.
34. Ceresa BP, Peterson JL. Cell and molecular biology of epidermal growth factor receptor. Int Rev Cell Mol Biol 2014;313:145–178. [PubMed: 25376492]
35. Guo W, Keckesova Z, Donaher JL, Shibue T, Tischler V, Reinhardt F, Itzkovitz S, et al. Slug and Sox9 cooperatively determine the mammary stem cell state. Cell 2012;148:1015–1028. [PubMed: 22385965]
36. Kang HM, Huang S, Reidy K, Han SH, Chinga F, Susztak K. Sox9-Positive Progenitor Cells Play a Key Role in Renal Tubule Epithelial Regeneration in Mice. Cell Rep 2016;14:861–871. [PubMed: 26776520]
37. Liu C, Liu L, Chen X, Cheng J, Zhang H, Shen J, Shan J, et al. Sox9 regulates self-renewal and tumorigenicity by promoting symmetrical cell division of cancer stem cells in hepatocellular carcinoma. Hepatology 2016;64:117–129. [PubMed: 26910875]
38. Ling S, Chang X, Schultz L, Lee TK, Chaux A, Marchionni L, Netto GJ, et al. An EGFR-ERK-SOX9 signaling cascade links urothelial development and regeneration to cancer. Cancer Res 2011;71:3812–3821. [PubMed: 21512138]
39. Liu F, Hon GC, Villa GR, Turner KM, Ikegami S, Yang H, Ye Z, et al. EGFR Mutation Promotes Glioblastoma through Epigenome and Transcription Factor Network Remodeling. Mol Cell 2015;60:307–318. [PubMed: 26455392]
40. Huang W, Beer RL, Delaspre F, Wang G, Edelman HE, Park H, Azuma M, et al. Sox9b is a mediator of retinoic acid signaling restricting endocrine progenitor differentiation. Dev Biol 2016;418:28–39. [PubMed: 27565026]
41. Natarajan A, Wagner B, Sibilia M. The EGF receptor is required for efficient liver regeneration (vol 104, pg 17081, 2007). Proceedings of the National Academy of Sciences of the United States of America 2007;104:19656–19656.
42. Lopez-Luque J, Caballero-Diaz D, Martinez-Palacian A, Roncero C, Moreno-Caceres J, Garcia-Bravo M, Grueso E, et al. Dissecting the Role of Epidermal Growth Factor Receptor Catalytic Activity During Liver Regeneration and Hepatocarcinogenesis. Hepatology 2016;63:604–619. [PubMed: 26313466]

43. Kitade M, Factor VM, Andersen JB, Tomokuni A, Kaji K, Akita H, Holczbauer A, et al. Specific fate decisions in adult hepatic progenitor cells driven by MET and EGFR signaling. Genes Dev 2013;27:1706–1717. [PubMed: 23913923]

44. Fuchs BC, Hoshida Y, Fujii T, Wei L, Yamada S, Lauwers GY, McGinn CM, et al. Epidermal growth factor receptor inhibition attenuates liver fibrosis and development of hepatocellular carcinoma. Hepatology 2014;59:1577–1590. [PubMed: 24677197]

45. Aguilar-Bravo B, Rodrigo-Torres D, Arino S, Coll M, Pose E, Blaya D, Graupera I, et al. Ductular Reaction Cells Display an Inflammatory Profile and Recruit Neutrophils in Alcoholic Hepatitis. Hepatology 2019;69:2180–2195. [PubMed: 30565271]

46. Planas-Paz L, Sun T, Pikiolek M, Cochran NR, Bergling S, Orsini V, Yang Z, et al. YAP, but Not RSPO-LGR4/5, Signaling in Biliary Epithelial Cells Promotes a Ductular Reaction in Response to Liver Injury. Cell Stem Cell 2019.

47. Boulter L, Govaere O, Bird TG, Radulescu S, Ramachandran P, Pellicoro A, Ridgway RA, et al. Macrophage-derived Wnt opposes Notch signaling to specify hepatic progenitor cell fate in chronic liver disease. Nature Medicine 2012;18:572–579.

48. Troiani T, Napolitano S, Della Corte CM, Martini G, Martinelli E, Morgillo F, Ciardiello F. Therapeutic value of EGFR inhibition in CRC and NSCLC: 15 years of clinical evidence. ESMO Open 2016;1:e000088. [PubMed: 27843640]

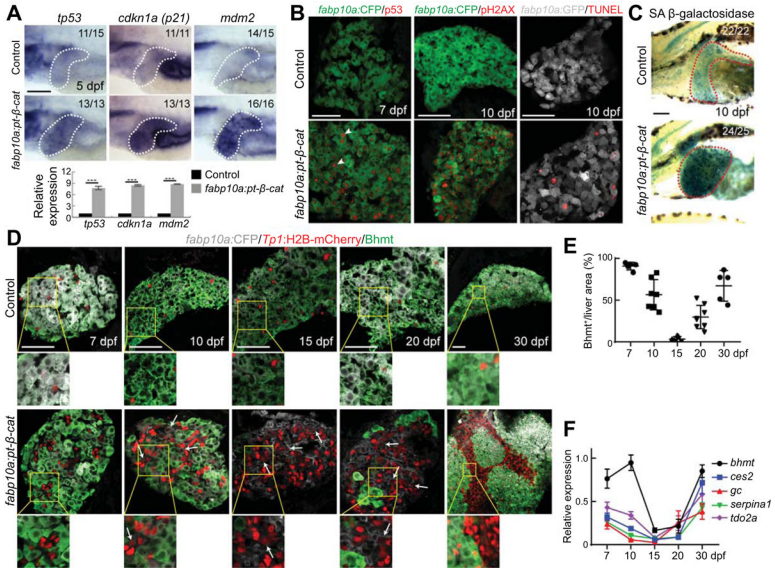

Figure 1. Hepatocyte-specific overexpression of an oncogene in zebrafish elicits liver damage followed by hepatocyte regeneration.

(**A**) Whole-mount in situ hybridization images show the hepatic expression of *tp53*, *cdkn1a (p21)*, and *mdm2* in control and *Tg(fabp10a:pt-β-catenin)* larvae at 5 dpf. Dotted lines outline livers. qPCR data show the relative expression levels of *tp53*, *cdkn1a*, and *mdm2* between *Tg(fabp10a:pt-b-catenin)* and control livers at 5 dpf. (**B**) Confocal images showing p53 (arrowheads) and *fabp10a*:CFP expression in 7-dpf livers, pH2AX and *fabp10a*:CFP expression in 10-dpf livers, and *fabp10a*:GFP expression and TUNEL labeling in 10-dpf livers. (**C**) β-galactosidase staining images showing senescence levels in 10-dpf *Tg(fabp10a:pt-b-catenin)* livers (dotted lines). (**D**) Confocal images showing the expression of *fabp10a*:CFP, *Tp1*:H2B-mCherry, and Bhmt in *Tg(fabp10a:pt-β-catenin)* and control livers. Boxed regions are enlarged below. Arrows point to LPCs. (**E**) Quantification of Bhmt-positive area in *Tg(fabp10a:pt-β-catenin)* livers. (**F**) qPCR data showing the relative expression levels of *bhmt*, *ces2*, *gc*, *serpina1*, and *tdo2a* between *Tg(fabp10a:pt-β-catenin)* and control livers. Scale bars, 200 μm (A, C), 50 μm (B, D). Numbers in the upper right corner indicate the proportion of larvae exhibiting the phenotype shown. Data are presented as mean ± s.d. (A, E) or ± s.e.m. (F). ***$P<0.001$; statistical significance was calculated using an unpaired two-tailed t-test.

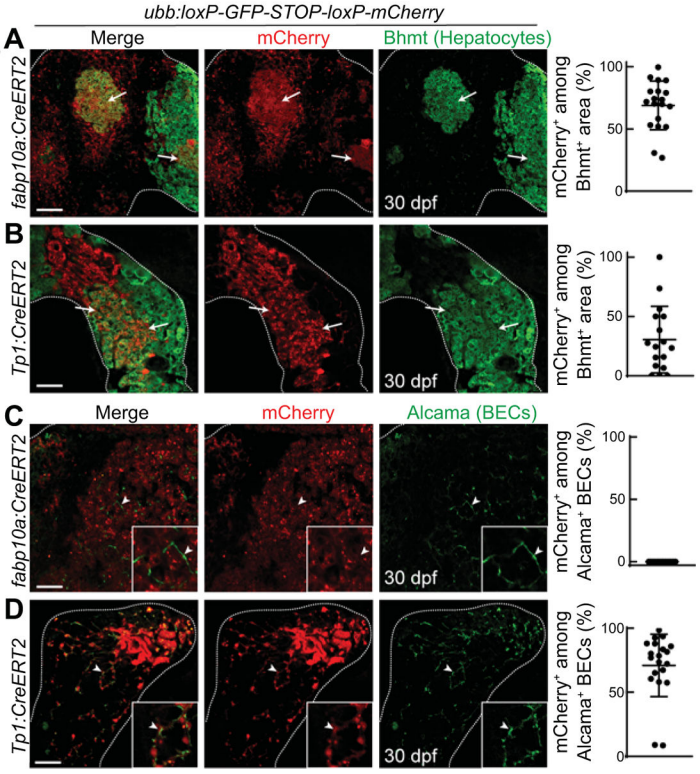

Figure 2. Both pre-existing hepatocytes and BECs contribute to regenerated hepatocytes in *Tg(fabp10a:pt-β-catenin)* zebrafish.

(**A, B**) Confocal images showing the expression of mCherry (lineage-traced cells) and Bhmt (hepatocytes) in *Tg(fabp10a:pt-β-catenin)* livers at 30 dpf. Quantification of the percentage of mCherry-positive area in Bhmt-positive liver area is shown.

(**C, D**) Confocal images showing the expression of mCherry (lineage-traced cells) and Alcama (BECs) in *Tg(fabp10a:pt-β-catenin)* livers at 30 dpf. Insets display enlarged regions. Quantification of the percentage of mCherry-positive BECs is shown. For Cre-mediated cell labeling, embryos/larvae were treated with 10 uM 4-OHT from 2.5 to 4 dpf for 36 hours. Arrows point to mCherry/Bhmt double-positive hepatocytes; arrowheads point to Alcama-positive BECs. Dotted lines outline livers. Scale bars, 50 μm. Data are presented as mean ± s.d.

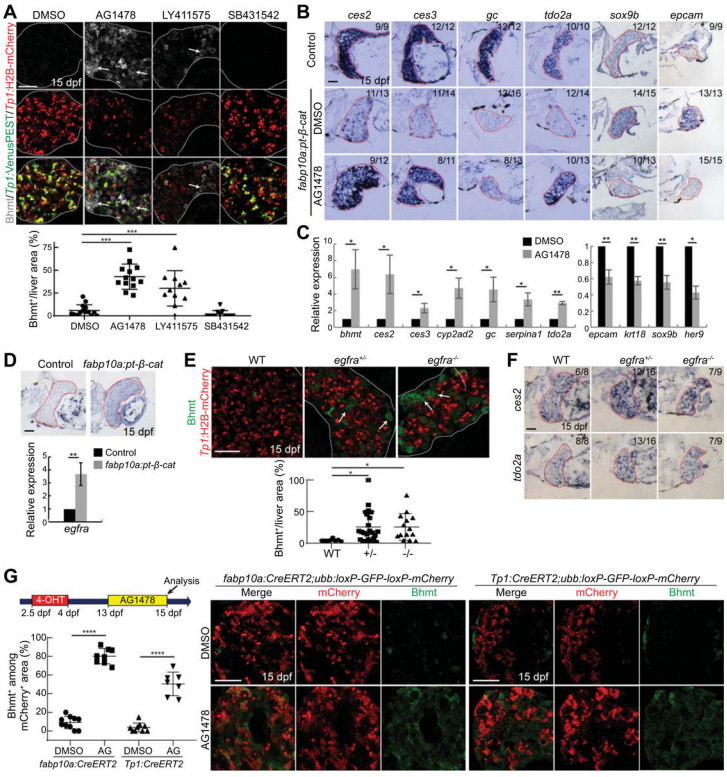

Figure 3. Suppressing EGFR signaling promotes LPC-to-hepatocyte differentiation.

(**A**) Confocal images showing the hepatic expression of Bhmt, *Tp1:*VenusPEST, and *Tp1:*H2B-mCherry in *Tg(fabp10a:pt-β-catenin)* larvae. Arrows point to Bhmt^{+} hepatocytes. Quantification of the percentage of Bhmt-positive liver area in *Tg(fabp10a:pt-β-catenin)* larvae is shown. (**B**) Section in situ hybridization images showing the expression of hepatocyte markers (*ces2*, *ces3*, *gc*, and *tdo2a*) and LPC/BEC markers (*sox9b* and *epcam*) in control and *Tg(fabp10a:pt-β-catenin)* larvae treated with DMSO or AG1478. Numbers in the upper right corner indicate the proportion of larvae exhibiting the phenotype shown. (**C**) qPCR data showing the relative expression levels of hepatocyte markers (*bhmt*, *ces2*, *ces3*, *cyp2ad2*, *gc*, *serpina1* and *tdo2a*) and LPC/BEC markers (*epcam*, *krt18*, *sox9b*, and *her9*) between DMSO- and AG1478-treated *Tg(fabp10a:pt-β-catenin)* livers at 15 dpf. (**D**) Section in situ hybridization images showing *egfra* expression in control and *Tg(fabp10a:pt-β-catenin)* livers at 15 dpf. qPCR data show the relative expression levels of *egfra* between control and *Tg(fabp10a:pt-β-catenin)* livers at 15 dpf. (**E**) Confocal images showing Bhmt (arrows) and *Tp1*:H2B-mCherry expression in *Tg(fabp10a:pt-β-catenin)* livers at 15 dpf. Quantification of Bhmt-positive area in *Tg(fabp10a:pt-β-catenin)* livers is shown. (**F**) Section in situ hybridization images showing the hepatic expression of *ces2* and *tdo2a* in 15-dpf *Tg(fabp10a:pt-β-catenin)* larvae. (**G**) Scheme illustrates 4-OHT and AG1478 treatments and analysis stage. Confocal images show the hepatic expression of Bhmt and mCherry (labeled cells) in 15-dpf *Tg(fabp10a:pt-β-catenin)* larvae. Hepatocyte- and BEC-derived LPCs were labeled with the *fabp10a:CreERT2* and *Tp1:CreERT2* lines, respectively, along with the Cre reporter line, *Tg(ubb:loxP-GFP-loxP-mCherry)*. The percentage of mCherry/Bhmt-double positive area in mCherry-positive area is quantified. Dotted lines outline livers; numbers in the upper right corner indicate the proportion of larvae exhibiting the phenotype

shown. Scale bars, 50 μm. Data are presented as mean ± s.d. *P<0.05, **P<0.01, ***P<0.001, ****P<0.0001; statistical significance was calculated using one-way ANOVA (A, E) or an unpaired two-tailed t-test (C, D, G).

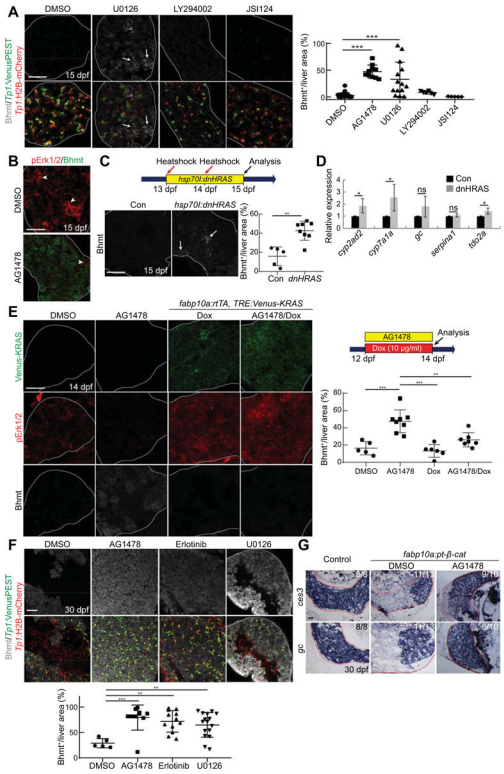

Figure 4. Suppression of MEK/ERK signaling promotes LPC-to-hepatocyte differentiation.

(**A**) Confocal images showing the hepatic expression of Bhmt, *Tp1:*VenusPEST, and *Tp1:*H2B-mCherry in 15-dpf *Tg(fabp10a:pt-β-catenin)* larvae treated with DMSO, U0126, LY294002, or JSI124 from 13 to 15 dpf. Quantification of the percentage of Bhmt-positive liver area is shown. (**B**) Confocal images showing the hepatic expression of pErk1/2 and Bhmt in 15-dpf *Tg(fabp10a:pt-β-catenin)* larvae. Arrowheads point to pErk1/2^{+} cells. (**C**) Confocal images showing Bhmt expression in *Tg(fabp10a:pt-β-catenin)* livers at 15 dpf. To block Ras activity, the animals were heat-shocked twice at 13 and 14 dpf. Quantification of the percentage of Bhmt-positive liver area is shown. (**D**) qPCR data showing the relative expression levels of hepatocyte markers (*cyp2ad2*, *cyp7a1a*, *gc*, *serpina1* and *tdo2a*) between *Tg(fabp10a:pt-β-catenin)* and *Tg(hsp70l:dnHRAS);Tg(fabp10a:pt-β-catenin)* livers at 15 dpf. (**E**) Confocal images showing the hepatic expression of Bhmt, pErk1/2, and Venus-KRAS in *Tg(fabp10a:pt-β-catenin)* larvae at 14 dpf. The *Tg(fabp10a:rtTA,TRE:Venus-KRAS)* line was used to overexpress KRAS. Scheme illustrates doxycycline (Dox) and AG1478 treatments and analysis stage. Quantification of the percentage of Bhmt-positive liver area is shown. (**F**) Confocal images showing the hepatic expression of Bhmt, *Tp1*:VenusPEST, and *Tp1*:H2B-mCherry in 30-dpf *Tg(fabp10a:pt-β-catenin)* larvae treated with AG1478, erlotinib, or U0126 from 13 to 15 dpf. Quantification of the percentage of Bhmt-positive liver area is shown. (**G**) Section in situ hybridization images showing the hepatic expression of *ces3* and *gc* in control and *Tg(fabp10a:pt-β-catenin)* larvae at 30 dpf. Numbers in the upper right corner indicate the proportion of larvae exhibiting the phenotype shown. Arrows point to Bhmt^{+} hepatocytes; dotted lines outline livers. Scale bars, 50 μm. Data are presented as mean ± s.d. **P*<0.05, ***P*<0.01, ****P*<0.001; statistical significance was calculated using one-way ANOVA (A, E, F) or an unpaired two-tailed t-test (C, D).

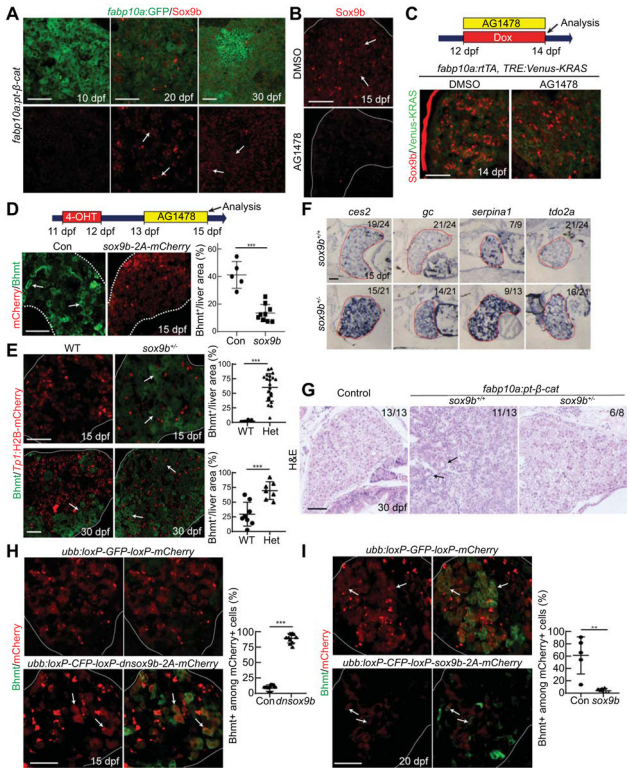

Figure 5. Sox9b suppresses LPC-to-hepatocyte differentiation.

(**A**) Confocal images showing the hepatic expression of *fabp10a*:GFP and Sox9b in *Tg(fabp10a:pt-β-catenin)* larvae. (**B**) Confocal images showing the hepatic expression of Sox9b in 15-dpf *Tg(fabp10a:pt-β-catenin)* larvae. Arrows point to Sox9b^{+} LPCs. (**C**) Scheme illustrates Dox and AG1478 treatments and analysis stage. Confocal images showing the hepatic expression of Sox9b and Venus-KRAS in *Tg(fabp10a:pt-β-catenin)* larvae at 14 dpf. The *Tg(fabp10a:rtTA,TRE:Venus-KRAS)* line was used to overexpress KRAS. (**D**) Scheme illustrates 4-OHT and AG1478 treatments and analysis stage. The *Tg(fabp10a:CreERT2)* and *Tg(ubb:loxP-GFP-loxP-sox9b-2A-mCherry)* lines were used to overexpress Sox9b in LPCs and hepatocytes. Confocal images showing the hepatic expression of Bhmt and mCherry (Sox9b-overexpressing cells) in 15-dpf *Tg(fabp10a:pt-β-catenin)* larvae. Arrows point to Bhmt-positive hepatocytes. Quantification of the percentage of Bhmt-positive liver area is shown. (**E**) Confocal images showing Bhmt and *Tp1:*H2B-mCherry expression in *Tg(fabp10a:pt-β-catenin)* livers at 15 and 30 dpf. Arrows point to Bhmt^{+} hepatocytes. Quantification of Bhmt-positive liver area is shown. (**F**) Section in situ hybridization images showing the expression of hepatocyte markers (*ces2*, *gc*, *serpina1* and *tdo2a*) in *sox9b*$^{+/+}$*;Tg(fabp10a:pt-β-catenin)* and *sox9b*$^{+/-}$*;Tg(fabp10a:pt-β-catenin)* livers at 15 dpf. (**G**) H&E staining images showing the histology of the liver at 30 dpf. Arrows point to dysplastic ducts. (**H, I**) Confocal images showing the expression of Bhmt and mCherry (dnSox9b- or Sox9b- overexpressing cells) in *Tg(fabp10a:pt-β-catenin)* larvae. The *Tg(ubb:loxP-CFP-loxP-sox9b-2A-mCherry)* and *Tg(ubb:loxP-CFP-loxP-dnsox9b-2A-mCherry)* lines were used to overexpress dnSox9b (H) and Sox9b (I), respectively, with the *Tg(fabp10a:CreERT2)* line; 4-OHT was administrated from 11 to 12 dpf. Quantification of the percentage of Bhmt^{+} cells among mCherry^{+} cells in the liver is shown. Arrows point to

Bhmt/mCherry double-positive cells. Dotted lines outline livers. Numbers in the upper right corner indicate the proportion of larvae exhibiting the phenotype shown. Scale bars, 50 μm. Data are presented as mean ± s.d. $^{**}P<0.01$, $^{***}P<0.001$; statistical significance was calculated using an unpaired two-tailed t-test.